Published in final edited form as:
Cancer Res. 2011 July 15; 71(14): 4758–4768. doi:10.1158/0008-5472.CAN-10-2527.

VEGF and c-Met Blockade Amplify Angiogenesis Inhibition in Pancreatic Islet Cancer

Weon-Kyoo You[1], **Barbara Sennino**[1], **Casey W. Williamson**[1], **Beverly Falcón**[1], **Hiroya Hashizume**[1], **Li-Chin Yao**[1], **Dana T. Aftab**[2], and **Donald M. McDonald**[1]

[1]Cardiovascular Research Institute, Comprehensive Cancer Center, and Department of Anatomy, University of California, San Francisco, California

[2]Exelixis Inc., South San Francisco, California

Abstract

Angiogenesis inhibitors that block vascular endothelial growth factor receptor (VEGFR) signaling slow the growth of many types of tumors, but eventually the disease progresses. Multiple strategies are being explored to improve efficacy by concurrent inhibition of other functionally relevant receptor tyrosine kinases (RTKs). XL880 (foretinib, GSK1363089) and XL184 (cabozantinib) are small molecule inhibitors that potently block multiple RTKs including VEGFR and the receptor of hepatocyte growth factor c-Met, which can drive tumor invasion and metastasis. This study compared the cellular effects of XL880 and XL184 to those of an RTK inhibitor (XL999) that blocks VEGFR but not c-Met. Treatment of RIP-Tag2 mice with XL999 resulted in 43% reduction in vascularity of spontaneous pancreatic islet tumors over 7 days, but treatment with XL880 or XL184 eliminated ~ 80% of the tumor vasculature, reduced pericytes and empty basement membrane sleeves, caused widespread intratumoral hypoxia and tumor cell apoptosis, and slowed regrowth of the tumor vasculature after drug withdrawal. Importantly, XL880 and XL184 also decreased invasiveness of primary tumors and reduced metastasis. Overall, these findings indicate that inhibition of c-Met and functionally related kinases amplifies the effects of VEGFR blockade and leads to rapid, robust, and progressive regression of tumor vasculature, increased intratumoral hypoxia and apoptosis, and reduced tumor invasiveness and metastasis.

Keywords

Angiogenesis inhibitors; c-Met; VEGF; receptor tyrosine kinases; XL880 (foretinib, GSK1363089); XL184 (cabozantinib); XL999; RIP-Tag2 mice

Introduction

Inhibitors of vascular endothelial growth factor (VEGF) signaling block VEGF-driven angiogenesis, prune VEGF-dependent blood vessels, and normalize vessels that do not regress (1–4). VEGF inhibitors can also promote tumor invasion and metastasis in some preclinical models (5, 6), but the underlying mechanism is still unclear (7, 8). Treatment of cancer patients with VEGF inhibitors can slow tumor growth and in some cases prolong survival, but resistance eventually develops and the disease progresses through growth of

Corresponding Author: Donald M. McDonald, Department of Anatomy, University of California, 513 Parnassus Avenue, Room S1363, San Francisco, CA 94143-0452. Phone: 415-476-2118; Fax: 415-476-4845; donald.mcdonald@ucsf.edu.

Disclosure of Potential Conflicts of Interest
Dana Aftab is employed by Exelixis Inc.

residual primary tumor or metastases (9–12). Inhibitors that target other pathways, such as those involved in tumor invasiveness, are therefore being developed (13, 14).

Hepatocyte growth factor (HGF, scatter factor), through its receptor c-Met (HGFR), is a potent motility factor and mitogen (15–18). HGF and c-Met are upregulated in many human cancers and contribute to tumor growth, angiogenesis, invasiveness, and metastasis (19, 20). Inhibition of the HGF/c-Met pathway can reduce tumor growth, angiogenesis, and metastasis in preclinical models (21–24).

c-Met expression is increased by hypoxia through activation of hypoxia inducible factor-1α (HIF-1α) and contributes to the aggressiveness of hypoxic tumors (25). HIF-1α-induced c-Met expression could be triggered by vascular pruning caused by VEGF inhibitors and could select for migratory, invasive tumor cells and predispose spread by metastasis (26). The strategic roles of VEGFR and c-Met signaling in tumor angiogenesis, invasion, and metastasis make these receptors attractive therapeutic targets (16–18, 27).

We examined the effects of two small-molecule RTK inhibitors, XL880 (foretinib, GSK1363089) and XL184 (cabozantinib), that block phosphorylation of c-Met and VEGFR at nanomolar or subnanomolar concentrations (27–29) to assess the interaction of these receptors in tumors. As set out in Table 1, both XL880 and XL184 block c-Met and VEGFR-2. In addition, XL880 inhibits AXL, Tie2, KIT, FLT3, PDGFR, and RON (27, 30, 31), and XL184 inhibits AXL, Tie2, KIT, FLT3, and RET but not PDGFR or RON (28, 29, 32). The lack of overlap of PDGFR and RON makes these receptors unlikely to explain the mutual effects of XL880 and XL184 on tumors.

The effects of a third RTK inhibitor, XL999, which blocks VEGFR, PDGFR, FGFR, FLT3, KIT, and AXL, was used for comparison because it does not block c-Met but does block many other targets of XL880 and XL184 (33, 34). Spontaneous pancreatic islet tumors in RIP-Tag2 transgenic mice were used as a model (4, 35, 36), and the abundance, cellular composition, and receptor expression of tumor blood vessels, intratumoral hypoxia, and measures of tumor aggressiveness were used as readouts.

Our studies revealed that XL880 or XL184, but not XL999, led to rapid, widespread, and progressive regression of tumor vasculature, extensive hypoxia and apoptosis of tumor cells, and decreased tumor aggressiveness.

Materials and Methods

Animals

RIP-Tag2 mice in a C57BL/6 background were used as the tumor model (35). All experiments were approved by the University of California, San Francisco Institutional Animal Care and Use Committee.

Treatments

RIP-Tag2 mice were 10-weeks old at the onset of treatment unless otherwise indicated. XL880 (foretinib, GSK1363089), XL184 (cabozantinib), and XL999 were suspended at a concentration of 5 mg/ml in sterile saline or water and administered by gavage daily for 7 days (see Supplemental Materials and Methods).

Detection of functional blood vessels and hypoxia

Functional blood vessels in tumors were identified and marked by FITC-labeled *Lycopersicon esculentum* lectin (LEA, 1 mg/ml, 100 μl, Vector Laboratories) injected via a tail vein (i.v.) 2 min before the perfusion of fixative (4). Hypoxic regions of tumors were

identified by pimonidazole hydrochloride (60 mg/kg, 2.5 μl/g of mouse body weight, Hypoxyprobe Plus Kit HP2, Chemicon) injected i.v. 1 hr before the perfusion (5).

Tissue fixation and immunohistochemistry

Mice were perfused through the heart with paraformaldehyde fixative (4, 36). Cryostat sections 80-μm in thickness were stained with combinations of the antibodies (see Supplemental Materials and Methods).

Imaging and analysis

Specimens were examined with a Zeiss Axiophot fluorescence microscope and a Zeiss LSM 510 laser scanning confocal microscope. Area densities of endothelial cells, pericytes, basement membrane, apoptotic cells and hypoxic regions were calculated from digital fluorescence microscopic images using an empirically determined threshold value of 30 to 50 (4, 36). Intensity of VEGFR-2, VEGFR-3, and E-cadherin immunofluorescence was measured (4, 36). Metastases of RIP-Tag2 tumors were identified in sections of liver stained for SV40 T-antigen. Vascularity of the trachea was expressed as the average number of capillaries that crossed cartilage rings (10 rings/mouse, 4–5 mice/group) (37).

Tumor size and Invasion index

The size of tumors in the pancreas from RIP-Tag2 mice treated with vehicle, XL880, or XL184 for 7 days (5 mice/group) was assessed in 80-μm sections stained for insulin or SV40 T-antigen and expressed as sectional area of tumor (4).

Invasion index was measured using ImageJ on fluorescence microscopic images (5× objective, 1× Optovar) of 80-μm sections of pancreas stained for insulin or SV40 T-antigen (red) and amylase (green channel). The red channel of RGB images was converted to 8-bit gray scale, and the tumor border was outlined using the freehand tool. Regions outside the tumor were filled black. A threshold in the range of 0 to 255 was applied to include all tumor cells, and then the image was converted to binary. Invasion index (values ≥ 1.0) was calculated from the area and perimeter of the tumor by the formula $1 / (4\pi * \text{Area}/\text{Perimeter}^2)$, where a circle has a value of 1.0. The median Invasion index was calculated for all tumors in each mouse (10–21 tumors/mouse). The mean Invasion index for each group was calculated from the median value for each mouse (4 mice/group).

Immunoprecipitation and Quantitative RT-PCR

Immunoprecipitation and qRT-PCR analysis were performed as described in Supplemental Materials and Methods.

Statistics

Values are expressed as means ± SE (4–6 mice/group). The significance of differences between groups was assessed by analysis of variance (ANOVA) followed by the Bonferroni-Dunn or Fisher test for multiple comparisons ($P < 0.05$ were considered significant).

Results

Massive regression of tumor vessels after XL880 or XL184

Blood vessels in RIP-Tag2 tumors were abundant, irregular, and tortuous under baseline conditions (Figure 1Ai) but were sparse after XL880 for 7 days (Figure 1Aii). Loss of tumor vessels was dose- and time-dependent. Reductions ranged from 40% at 10 mg/kg to 80% at 60 mg/kg (Figure 1Aiii). Time-course studies revealed no reduction at 6 hours, 40%

reduction at 1 day, 76% at 7 days, and 90% at 14 days (Figure 1Bi–iv). Tumor vascularity decreased after XL184 (Figure 1Ci–ii), with reductions ranging from 67% at 3 mg/kg to 83% at 30 mg/kg for 7 days (Figure 1Ciii).

XL999, which inhibits VEGFR but not c-Met, reduced the vascularity of RIP-Tag2 tumors, but the magnitude of the reduction at 7 days (43%) was significantly less than after XL880 (80%) or XL184 (77%) (Figure 1Di), and the surviving blood vessels were different. After XL880 or XL184 for 7 days or longer, many remaining tumor vessels were narrow, variable in diameter, and appeared fragmented (Figure 1Dii). By contrast, most tumor vessels present after XL999 for 7 days were larger, more uniform in caliber ("normalized"), and had less branching and fewer sprouts than present under baseline conditions (Figure 1Diii). Because of evidence that some capillaries of normal organs regress after VEGF inhibition (4, 38, 39), we investigated this effect of XL880 and found consistent reductions in the number of capillaries in the trachea, thyroid, choriocapillaris of the eye, and jejunum (Supplemental Figure 1).

Reduction in VEGFR-2 and VEGFR-3

Strong and widespread VEGFR-2 immunoreactivity highlighted the dense vascularity of RIP-Tag2 tumors under baseline conditions (Figure 2Ai) but was conspicuously reduced after XL880 (Figure 2Aii). Overall VEGFR-2 immunoreactivity was reduced 93% after the 7-day treatment (Figure 2Aiii). The speed of the change was evident in the 86% reduction in expression of VEGFR-2 mRNA after only 1 day (Figure 2Aiv).

VEGFR-3 immunoreactivity was also strong and widespread on tumor vessels and was sharply reduced by XL880 for 7 days (Figure 2Bi–ii). Overall VEGFR-3 immunoreactivity was reduced 94% at 7 days (Figure 2Aiii), which was obvious in blood vessels but did not occur in peritumoral lymphatics (Figure 2Bii, arrows). Expression of VEGFR-3 mRNA was reduced by 80% after only 1 day (Figure 2Aiv).

The large reductions in VEGFR-2 and VEGFR-3 immunoreactivities in treated tumors (Figure 2Aiii) resulted from two changes: (i) decreased vascularity, reflected by the reduction in number of tumor vessels (Figure 2Aii, 2Bii), and (ii) decreased receptor protein in the surviving tumor vessels, reflected by the dose-dependent decrease in brightness of immunofluorescence (Figure 2Biii–iv). Because of this dual effect, the reductions in overall VEGFR-2 and VEGFR-3 immunoreactivity and expression were significantly greater than the corresponding reductions in CD31 (Figure 2Aiii–iv).

Impaired function of surviving tumor vessels

Blood vessel function was assessed by i.v. injection of FITC-labeled LEA lectin, which uniformly stains the luminal surface of the endothelium of perfused blood vessels (4). Under baseline conditions, the pattern of lectin staining in tumors largely matched the distribution of CD31 staining (Figure 2Ci–Cii), indicating that most vessels were functional. After XL880 for 7 days, tumor vascularity was markedly reduced, and lectin staining was absent in some of the remaining vessels (Figure 2Ciii–iv, arrows), indicative of impaired functionality, or was discontinuous (Figure 2Di) in vessels that had discontinuous staining for CD31 and type IV collagen (Figure 2Dii–iii), consistent with vessels undergoing regression.

Reduction in pericytes and empty basement membrane sleeves

NG2-positive pericytes were abundant throughout RIP-Tag2 tumors under baseline conditions (Figure 3Ai) but were sparse after XL880 or XL184 for 7 days (Figure 3Aii–iii). Measurements showed a 71% reduction in NG2 immunoreactivity after the highest dose of

XL880 (Figure 3Bi), which was almost as large as the corresponding 80% reduction in CD31 (Figure 1Aiii). The abnormally loose association of pericytes with tumor blood vessels was prominent under baseline conditions (Figure 3Bii) and was still evident after XL880 (Figure 3Biii).

Type IV collagen immunoreactivity largely matched the CD31 staining of blood vessels in tumors at baseline (Figure 3Ci–ii). The amount of type IV collagen was reduced after XL880 for 7 days (Figure 3Ciii), but not as much as CD31 staining (Figure 3Civ). Measurements showed a 52% reduction in type IV collagen compared to the 80% reduction in CD31 (Figure 3Di).

The number of empty basement membrane sleeves was reflected by the discrepancy between the loss of endothelial cells and the loss of basement membrane (Figure 3Di). After XL880 for 7 days, about 20% of the original amount of basement membrane was on surviving tumor vessels, 28% was in the form of empty sleeves, and 52% was lost. Vascular basement membrane was similarly reduced after XL184 (Figure 3Dii–iii).

Regrowth of tumor vasculature

Stopping XL880 after treatment for 7 days was followed by partial regrowth of the tumor vasculature over the subsequent 7 days, but tumor vascularity did not return to the baseline (Supplementary Figure 2Ai–iv). With the 77% reduction in vascularity after the 7-day treatment as a reference, recovery was 22% (58% below baseline) at 2 days and was 51% (29% below baseline) at 7 days (Supplementary Figure 2Bi). Consistent with continuing regrowth, endothelial cell sprouts were still present at 7 days (Supplementary Figure 2Bii).

Recovery of the intensity of VEGFR-2 immunofluorescence of tumor vessels was not similarly delayed. Brightness of VEGFR-2 immunofluorescence was 54% less than baseline after XL880 for 7 days but was only 21% less at 2 days and was back to baseline at 7 days (Supplementary Figure 2Biii). Similarly, hypoxic regions of tumors marked by pimonidazole staining rapidly decreased after XL880 was withdrawn and were not present at 7 days after treatment ended (Supplementary Figure 2Ci–iv).

Distribution of c-Met in tumors

Under baseline conditions, the pattern of c-Met immunoreactivity was largely vascular (Figure 4Ai). About 7% of blood vessels in RIP-Tag2 tumors were stained. Vascular staining for c-Met was much less after XL880 (Figure 4Aii) or XL184 (Figure 4Aiii) but was not noticeably different after XL999 for 7 days (Figure 4Aiv). Colocalization with CD31 staining confirmed the association of most c-Met immunoreactivity with endothelial cells (Figure 4Bi–iv). Surface plots of c-Met immunofluorescence of baseline tumors showed that the vascular pattern was surrounded by weak, uniform background fluorescence in regions where tumor cells predominated (Figure 4Ci). In contrast, surface plots of tumors after XL880 or XL184 lacked the vascular pattern but still had the weak background fluorescence (Figure 4Cii–iii). Neither the amount nor the distribution of c-Met immunoreactivity changed appreciably after XL999 (Figure 4Civ). Colocalization of faint c-Met immunoreactivity with staining for SV40 T-antigen was consistent with weak c-Met expression in some tumor cells under baseline conditions (Figure 4Di).

Pixels where c-Met immunoreactivity colocalized with CD31 decreased by at least half after XL880 or XL184, suggestive of a preferential effect on endothelial cells (Figure 4Dii). This was not found after XL999.

Overall c-Met protein in tumors assessed by immunoprecipitation was slightly less after XL184, but phosphorylated c-Met was markedly reduced after XL184 for 7 days (Figure 4Diii). Neither changed after XL999 (Figure 4Diii).

Intratumoral hypoxia and apoptosis

Hypoxic regions marked by pimonidazole staining were sparse or absent in tumors of 10-or 11-week old RIP-Tag2 mice treated with vehicle (Figure 5Ai) but were abundant and conspicuous in tumors after XL880 or XL184 for 7 days (Figure 5Aii–iii). Surface plots highlighted the difference between negligible pimonidazole immunofluorescence in vehicle-treated tumors and the strong, widespread staining after XL880 (Figure 5Bi). Pimonidazole staining was increased about 100-fold, from 11% of tumor area after XL880 and 9% after XL184, compared to the baseline value of only 0.1% (Figure 5Bii).

After XL880 or XL184, most pimonidazole staining was in regions of tumors that were avascular or had narrowed blood vessels (Figure 5Aii–iii). Many pimonidazole-positive regions were separated from blood vessels by sleeves of unstained tumor cells (average width 36 ± 3 μm, Figure 5Biii). Pimonidazole staining next to narrowed or fragmented tumor vessels did not have an intervening sleeve of unstained cells (Figure 5Biii).

Apoptotic cells identified by activated caspase-3 immunoreactivity were scattered in baseline tumors (Figure 5Ci). After XL880 or XL184, activated caspase-3 immunoreactivity was much more extensive and was associated with clumps of cells (Figure 5Cii). The fractional area of activated caspase-3 increased 5-fold after the highest dose of XL880 for 7 days (Figure 5Ciii). Some activated caspase-3 immunoreactivity coincided with CD31 staining, indicative of apoptotic endothelial cells (Figure 5Di). Activated caspase-3 staining after XL184 resembled that after XL880 (Figure 5Cii, Dii), but after XL999 the staining resembled that found in baseline tumors (Figure 5Ci, Diii).

Tumor aggressiveness

As indices of aggressiveness of RIP-Tag2 tumors, we examined tumor shape, E-cadherin staining, size, and metastasis to the liver. The contour of the tumor perimeter was assessed in sections stained for insulin or SV40 T-antigen in tumor cells and amylase in the surrounding acinar pancreas. Vehicle-treated tumors had irregular borders (Figure 6Ai–ii), but tumors treated with XL880 for 14 days had a smooth contour and distinct margin with the neighboring acinar pancreas (Figure 6Aiii–iv). The irregularity of the tumor border, quantified as the Invasion index, was significantly less (3.4) after XL880 for 14 days than after vehicle (5.4) (Figure 6Bi–iii).

E-cadherin immunoreactivity of tumor cells, as an indicator of epithelial-mesenchymal transition (EMT) status (40), was faint to absent under baseline conditions (Supplementary Figure 2Di), but was stronger after XL880 or XL184 for 7 days (Supplementary Figure 2Dii–iii). The mean intensity of E-cadherin immunofluorescence increased from 32 in vehicle-treated tumors to 41 after XL880 and 46 after XL184 for 7 days (Supplementary Figure 2Div). The acinar pancreas and pancreatic ducts had strong E-cadherin immunoreactivity in under all conditions.

Tumors in RIP-Tag2 mice treated for 7 days beginning at age 10 weeks were 40% smaller after XL880 and 35% smaller after XL184, compared to corresponding values for vehicle (Figure 6Ci).

Tumor cells, identified by SV40 T-antigen immunofluorescence, were scattered in histological sections of liver from 3 out of 4 RIP-Tag2 mice treated with vehicle for 14 days

(Figure 6Cii), but none were found in livers of 4 mice treated with XL880 for the same period (Figure 6Ciii).

To determine whether RIP-Tag2 tumors become more invasive after XL880 is withdrawn, we treated mice with XL880 for 7 days, from age 10 to 11 weeks, and then studied them 7 or 14 days later. The border of tumors was irregular at baseline but was much smoother after XL880 for 7 days (Figure 6Di–ii). At 7 days after treatment ended, the tumor border was still smooth, but small groups of tumor cells projected into the surrounding acinar pancreas (Figure 6Diii). At 14 days, tumors had irregular borders similar to but not greater than those at baseline (Figure 6Di and Div). Measurements of Invasion index reflected these changes (Figure 6Dv).

Discussion

The overall goal of this study was to determine the cellular effects of two small molecule RTK inhibitors, XL880 and XL184, that block key signaling pathways involved in angiogenesis and tumor invasiveness. Both inhibitors target VEGFR and c-Met at low nanomolar or subnanomolar concentrations together with several other RTKs, and both had rapid, robust, profound, and largely similar cellular effects on blood vessels and tumor cells of RIP-Tag2 tumors. These effects differed qualitatively and quantitatively from those found after treatment with XL999, an RTK inhibitor that does not target c-Met but does block VEGFR plus multiple other receptors blocked by XL880 and XL184.

Treatment with XL880 or XL184 led to rapid and severe changes in tumor blood vessels, which were greater than after XL999 over a similar dosage range or after other VEGF inhibitors (4, 36, 41). VEGFR-2 and VEGFR-3 proteins and their respective mRNA expression were reduced even more than corresponding values for CD31, consistent with dual effects of vessel regression and downregulation of expression on the remaining tumor vessels (4, 36).

Selective inhibition of VEGF signaling causes regression of some tumor vessels, but those that remain tend to be more normal (3, 4), which were confirmed after XL999. However, surviving tumor vessels were qualitatively different after XL880 or XL184, which were narrow, fragmented, and not stained by intravenous FITC-LEA lectin, suggestive of continuing regression (4, 36, 41). The tumor vascularity continued to decrease during the second week of XL880 treatment. This progressive change differs from vascular regression due to many selective VEGF inhibitors, which tends to plateau after a week or so as tumor vessels normalize (3, 4).

Basement membrane sleeves and pericytes were decreased after treatment with XL880 or XL184. Some reduction was also found with XL999, as has been reported for other VEGF inhibitors (4, 36, 41), but the decrease was less. Basement membrane sleeves depend in part on the viability of the associated endothelial cells and/or pericytes, but they were not lost proportionally: endothelial cells were reduced 80%, pericytes 71%, and basement membrane only 52%.

Tumor vessels rapidly regrow after withdrawal of VEGF inhibitors (36). Tumor vessels also regrew after withdrawal of XL880 or XL184, but the regrowth was slowed. Although the mechanism is uncertain, one factor for the reduced vascular regrowth after XL880 or XL184 may be the greater loss of pericytes and basement membrane sleeves that provide a scaffold for regrowing blood vessels (36).

To better understand the robust effects of XL880 and XL184 on blood vessels in RIP-Tag2 tumors, we examined the amount and distribution of c-Met immunoreactivity. Strong

staining for c-Met was consistently found in some tumor vessels at baseline. Colocalization with CD31 indicated the vascular staining of c-Met was restricted to endothelial cells. In addition, some tumor cells marked by SV40 T-antigen had faint c-Met immunoreactivity. Vascular staining for c-Met was conspicuously less after XL880 or XL184 but was unchanged after XL999. Consistent with this finding, total c-Met and phosphorylated c-Met, assessed by immunoprecipitation, were both reduced after XL184, but neither was significantly reduced after XL999. Based on intensity of c-Met immunoreactivity, vascular endothelial cells probably made a significant contribution to the signal in the immunoblots and were targets of XL880 and XL184, but the presence of weak staining in tumor cells indicates that c-Met blockade is also likely to have direct effects on tumor cells in the RIP-Tag2 model.

The robust effects of XL880 and XL184 on RIP-Tag2 tumors were not limited to tumor vessels. Intratumoral hypoxia and tumor cell apoptosis were also widespread. Induction of hypoxia and apoptosis was probably due to the extensive and progressive pruning of tumor vessels without vessel normalization. The association of pimonidazole staining with regions of tumor that had few or no blood vessels is consistent with this interpretation.

Invasiveness, which is a typical feature of aggressive tumors (42, 43), increases in some preclinical models after inhibition of VEGF (5, 6, 44, 45). Treatment with XL880 resulted in smaller and less invasive tumors in RIP-Tag2 mice, and importantly, recovery of tumor invasiveness was slowed and did not rebound at an exaggerated rate during the first two weeks after XL880 was withdrawn.

The involvement of c-Met in the anti-invasive action of XL880 and XL184 is consistent with their potent inhibitory actions on c-Met, the presence of c-Met immunoreactivity in RIP-Tag2 tumors under baseline conditions, and the reduction in c-Met and invasiveness after treatment. XL880 and XL184 had IC_{50} values for c-Met of 0.4 and 1.3 nM, compared to 463 nM for XL999. Involvement of c-Met also fits with the reduction in phospho-c-Met protein in the tumors after treatment with XL184. XL999 lacked the robust effect of XL880 and XL184 on apoptosis of blood vessels and tumor cells in RIP-Tag2 tumors. Although inhibition of AXL could contribute to the anti-invasive action, as reported in other models (46–49), this is unlikely to be the main target because XL880, XL184, and XL999 block AXL about equally, with IC_{50} values in the range of 4.6–11 nM.

The kinase profiles of XL880, XL184, and XL999 had differences in addition to c-Met, and drug efficacy is also influenced by in vivo absorption, stability, clearance, and other chemical properties that influence pharmacokinetics and pharmacodynamics. Therefore, confirmation of essential or exclusive roles of inhibition of c-Met and VEGFR in the anti-invasive effects of XL880 and XL184 will require the use of more selective inhibitors, comparison of drug actions after genetic deletion of c-Met, or other strategies that target these signaling pathways without impacting other receptors.

In conclusion, we found that XL880 and XL184 caused rapid and extensive regression of endothelial cells and pericytes of blood vessels in RIP-Tag2 tumors. Regression of the tumor vasculature was widespread, progressive, and accompanied by extensive intratumoral hypoxia and apoptosis of tumor cells. The treated tumors were smaller, less invasive, and accompanied by fewer liver metastases. The findings are consistent with the distinctive anti-tumoral actions of XL880 and XL184 resulting from inhibition of VEGFR and c-Met together. However, inhibition of other receptors and chemical properties that influence pharmacokinetics and pharmacodynamics could also contribute. Careful assessment using strategies for selective inhibition or knockdown of individual receptors or pathways will be

necessary to determine whether inhibition of VEGFR and c-Met is necessary and sufficient to reproduce all of the robust effects of XL880 and XL184 on tumors.

Supplementary Material

Refer to Web version on PubMed Central for supplementary material.

Acknowledgments

We thank Rolf Brekken of the University of Texas Southwestern Medical Center for the VEGFR-2 antibody, Peter Baluk, and Christophe Colas for valuable advice and discussions, and Jie Wei for genotyping the mice.

Grant Support

National Institutes of Health grants HL24136 and HL59157 from the National Heart, Lung, and Blood Institute; CA82923 from the National Cancer Institute; a grant from Exelixis Inc.; and funding from AngelWorks Foundation to DMcD.

References

1. Ferrara N, Chen H, Davis-Smyth T, et al. Vascular endothelial growth factor is essential for corpus luteum angiogenesis. Nat Med. 1998; 4:336–340. [PubMed: 9500609]
2. Brekken RA, Overholser JP, Stastny VA, Waltenberger J, Minna JD, Thorpe PE. Selective inhibition of vascular endothelial growth factor (VEGF) receptor 2 (KDR/Flk-1) activity by a monoclonal anti-VEGF antibody blocks tumor growth in mice. Cancer Res. 2000; 60:5117–5124. [PubMed: 11016638]
3. Jain RK. Normalizing tumor vasculature with anti-angiogenic therapy: a new paradigm for combination therapy. Nat Med. 2001; 7:987–989. [PubMed: 11533692]
4. Inai T, Mancuso M, Hashizume H, et al. Inhibition of vascular endothelial growth factor (VEGF) signaling in cancer causes loss of endothelial fenestrations, regression of tumor vessels, and appearance of basement membrane ghosts. Am J Pathol. 2004; 165:35–52. [PubMed: 15215160]
5. Paez-Ribes M, Allen E, Hudock J, et al. Antiangiogenic therapy elicits malignant progression of tumors to increased local invasion and distant metastasis. Cancer Cell. 2009; 15:220–231. [PubMed: 19249680]
6. Ebos JM, Lee CR, Cruz-Munoz W, Bjarnason GA, Christensen JG, Kerbel RS. Accelerated metastasis after short-term treatment with a potent inhibitor of tumor angiogenesis. Cancer Cell. 2009; 15:232–239. [PubMed: 19249681]
7. Hayden EC. Cutting off cancer's supply lines. Nature. 2009; 458:686–687. [PubMed: 19360048]
8. Loges S, Mazzone M, Hohensinner P, Carmeliet P. Silencing or fueling metastasis with VEGF inhibitors: antiangiogenesis revisited. Cancer Cell. 2009; 15:167–170. [PubMed: 19249675]
9. Goodman VL, Rock EP, Dagher R, et al. Approval summary: sunitinib for the treatment of imatinib refractory or intolerant gastrointestinal stromal tumors and advanced renal cell carcinoma. Clin Cancer Res. 2007; 13:1367–1373. [PubMed: 17332278]
10. Rock EP, Goodman V, Jiang JX, et al. Food and Drug Administration drug approval summary: Sunitinib malate for the treatment of gastrointestinal stromal tumor and advanced renal cell carcinoma. Oncologist. 2007; 12:107–113. [PubMed: 17227905]
11. Cohen MH, Gootenberg J, Keegan P, Pazdur R. FDA drug approval summary: bevacizumab (Avastin) plus Carboplatin and Paclitaxel as first-line treatment of advanced/metastatic recurrent nonsquamous non-small cell lung cancer. Oncologist. 2007; 12:713–718. [PubMed: 17602060]
12. Bergers G, Hanahan D. Modes of resistance to anti-angiogenic therapy. Nat Rev Cancer. 2008; 8:592–603. [PubMed: 18650835]
13. Ferrara N, Kerbel RS. Angiogenesis as a therapeutic target. Nature. 2005; 438:967–974. [PubMed: 16355214]
14. de Jonge MJ, Verweij J. Multiple targeted tyrosine kinase inhibition in the clinic: all for one or one for all? Eur J Cancer. 2006; 42:1351–1356. [PubMed: 16740386]

15. Bussolino F, Di Renzo MF, Ziche M, et al. Hepatocyte growth factor is a potent angiogenic factor which stimulates endothelial cell motility and growth. J Cell Biol. 1992; 119:629–641. [PubMed: 1383237]
16. Benvenuti S, Comoglio PM. The MET receptor tyrosine kinase in invasion and metastasis. J Cell Physiol. 2007; 213:316–325. [PubMed: 17607709]
17. Christensen J, Anderes K. Beyond VEGF: targeting tumor growth and angiogenesis via alternative mechanisms. Adv Exp Med Biol. 2008; 610:43–53. [PubMed: 18593014]
18. Cecchi F, Rabe DC, Bottaro DP. Targeting the HGF/Met signalling pathway in cancer. Eur J Cancer. 2010; 46:1260–1270. [PubMed: 20303741]
19. To CT, Tsao MS. The roles of hepatocyte growth factor/scatter factor and met receptor in human cancers (Review). Oncol Rep. 1998; 5:1013–1024. [PubMed: 9683803]
20. Birchmeier C, Birchmeier W, Gherardi E, Vande Woude GF. Met, metastasis, motility and more. Nat Rev Mol Cell Biol. 2003; 4:915–925. [PubMed: 14685170]
21. Kuba K, Matsumoto K, Date K, Shimura H, Tanaka M, Nakamura T. HGF/NK4, a four-kringle antagonist of hepatocyte growth factor, is an angiogenesis inhibitor that suppresses tumor growth and metastasis in mice. Cancer Res. 2000; 60:6737–6743. [PubMed: 11118060]
22. Christensen JG, Schreck R, Burrows J, et al. A selective small molecule inhibitor of c-Met kinase inhibits c-Met-dependent phenotypes in vitro and exhibits cytoreductive antitumor activity in vivo. Cancer Res. 2003; 63:7345–7355. [PubMed: 14612533]
23. Michieli P, Mazzone M, Basilico C, et al. Targeting the tumor and its microenvironment by a dual-function decoy Met receptor. Cancer Cell. 2004; 6:61–73. [PubMed: 15261142]
24. Martens T, Schmidt NO, Eckerich C, et al. A novel one-armed anti-c-Met antibody inhibits glioblastoma growth in vivo. Clin Cancer Res. 2006; 12:6144–6152. [PubMed: 17062691]
25. Pennacchietti S, Michieli P, Galluzzo M, Mazzone M, Giordano S, Comoglio PM. Hypoxia promotes invasive growth by transcriptional activation of the met protooncogene. Cancer Cell. 2003; 3:347–361. [PubMed: 12726861]
26. Bottaro DP, Liotta LA. Cancer: Out of air is not out of action. Nature. 2003; 423:593–595. [PubMed: 12789320]
27. Qian F, Engst S, Yamaguchi K, et al. Inhibition of tumor cell growth, invasion, and metastasis by EXEL-2880 (XL880, GSK1363089), a novel inhibitor of HGF and VEGF receptor tyrosine kinases. Cancer Res. 2009; 69:8009–8016. [PubMed: 19808973]
28. Salgia R, Hong DS, Camacho LH, et al. A phase I dose-escalation study of the safety and pharmacokinetics (PK) of XL184, a VEGFR and MET kinase inhibitor, administered orally to patients (pts) with advanced malignancies. J Clin Oncol. 2007; 25:14031.
29. Salgia R, Sherman S, Hong DS, et al. A phase I study of XL184, a RET, VEGFR2, and MET kinase inhibitor, in patients (pts) with advanced malignancies, including pts with medullary thyroid cancer (MTC). J Clin Oncol. 2008; 26:3522.
30. Bean J, Brennan C, Shih JY, et al. MET amplification occurs with or without T790M mutations in EGFR mutant lung tumors with acquired resistance to gefitinib or erlotinib. Proc Natl Acad Sci U S A. 2007; 104:20932–20937. [PubMed: 18093943]
31. Liu L, Greger J, Shi H, et al. Novel mechanism of lapatinib resistance in HER2-positive breast tumor cells: activation of AXL. Cancer Res. 2009; 69:6871–6878. [PubMed: 19671800]
32. Joly AH. Simultaneous blockade of VEGF and HGF receptors results in potent anti-angiogenic and anti-tumor effects. Eur J Cancer. 2006; Suppl 4:35. (Abstract 104).
33. Cripe L, McGuire W, Wertheim M, et al. Integrated report of the phase 2 experience with XL999 administered IV to patients (pts) with NSCLC, renal cell CA (RCC), metastatic colorectal CA (CRC), recurrent ovarian CA, acute myelogenous leaukemia (AML), and multiple myeloma (MM). J Clin Oncol. 2007; 25:3591.
34. Aftab D. The spectrum-selective kinase inhibitor EXEL-0999 inhibits mitogenic and angiogenic kinases, and causes rapid tumor vasculature destruction and regression in mouse xenograft models. Eur J Cancer. 2004 Suppl. 2:141.
35. Hanahan D. Heritable formation of pancreatic beta-cell tumours in transgenic mice expressing recombinant insulin/simian virus 40 oncogenes. Nature. 1985; 315:115–122. [PubMed: 2986015]

36. Mancuso MR, Davis R, Norberg SM, et al. Rapid vascular regrowth in tumors after reversal of VEGF inhibition. J Clin Invest. 2006; 116:2610–2621. [PubMed: 17016557]
37. Baffert F, Thurston G, Rochon-Duck M, Le T, Brekken R, McDonald DM. Age-related changes in vascular endothelial growth factor dependency and angiopoietin-1-induced plasticity of adult blood vessels. Circ Res. 2004; 94:984–992. [PubMed: 15001532]
38. Baffert F, Le T, Sennino B, et al. Cellular changes in normal blood capillaries undergoing regression after inhibition of VEGF signaling. Am J Physiol Heart Circ Physiol. 2006; 290:H547–H559. [PubMed: 16172161]
39. Kamba T, Tam BY, Hashizume H, et al. VEGF-dependent plasticity of fenestrated capillaries in the normal adult microvasculature. Am J Physiol Heart Circ Physiol. 2006; 290:H560–H576. [PubMed: 16172168]
40. von Burstin J, Eser S, Paul MC, et al. E-cadherin regulates metastasis of pancreatic cancer in vivo and is suppressed by a SNAIL/HDAC1/HDAC2 repressor complex. Gastroenterology. 2009; 137:361–371. [PubMed: 19362090]
41. Nakahara T, Norberg SM, Shalinsky DR, Hu-Lowe DD, McDonald DM. Effect of inhibition of vascular endothelial growth factor signaling on distribution of extravasated antibodies in tumors. Cancer Res. 2006; 66:1434–1445. [PubMed: 16452199]
42. Bergers G, Brekken R, McMahon G, et al. Matrix metalloproteinase-9 triggers the angiogenic switch during carcinogenesis. Nat Cell Biol. 2000; 2:737–744. [PubMed: 11025665]
43. Joyce JA, Baruch A, Chehade K, et al. Cathepsin cysteine proteases are effectors of invasive growth and angiogenesis during multistage tumorigenesis. Cancer Cell. 2004; 5:443–453. [PubMed: 15144952]
44. Casanovas O, Hicklin DJ, Bergers G, Hanahan D. Drug resistance by evasion of antiangiogenic targeting of VEGF signaling in late-stage pancreatic islet tumors. Cancer Cell. 2005; 8:299–309. [PubMed: 16226705]
45. Du R, Lu KV, Petritsch C, et al. HIF1alpha induces the recruitment of bone marrow-derived vascular modulatory cells to regulate tumor angiogenesis and invasion. Cancer Cell. 2008; 13:206–220. [PubMed: 18328425]
46. Li Y, Ye X, Tan C, et al. Axl as a potential therapeutic target in cancer: role of Axl in tumor growth, metastasis and angiogenesis. Oncogene. 2009; 28:3442–3455. [PubMed: 19633687]
47. Holland SJ, Pan A, Franci C, et al. R428, a selective small molecule inhibitor of Axl kinase, blocks tumor spread and prolongs survival in models of metastatic breast cancer. Cancer Res. 2010; 70:1544–1554. [PubMed: 20145120]
48. Ye X, Li Y, Stawicki S, et al. An anti-Axl monoclonal antibody attenuates xenograft tumor growth and enhances the effect of multiple anticancer therapies. Oncogene. 2010; 29:5254–5264. [PubMed: 20603615]
49. Gjerdrum C, Tiron C, Hoiby T, et al. Axl is an essential epithelial-to-mesenchymal transition-induced regulator of breast cancer metastasis and patient survival. Proc Natl Acad Sci U S A. 2010; 107:1124–1129. [PubMed: 20080645]
50. Wilhelm S, Carter C, Lynch M, et al. Discovery and development of sorafenib: a multikinase inhibitor for treating cancer. Nat Rev Drug Discov. 2006; 5:835–844. [PubMed: 17016424]

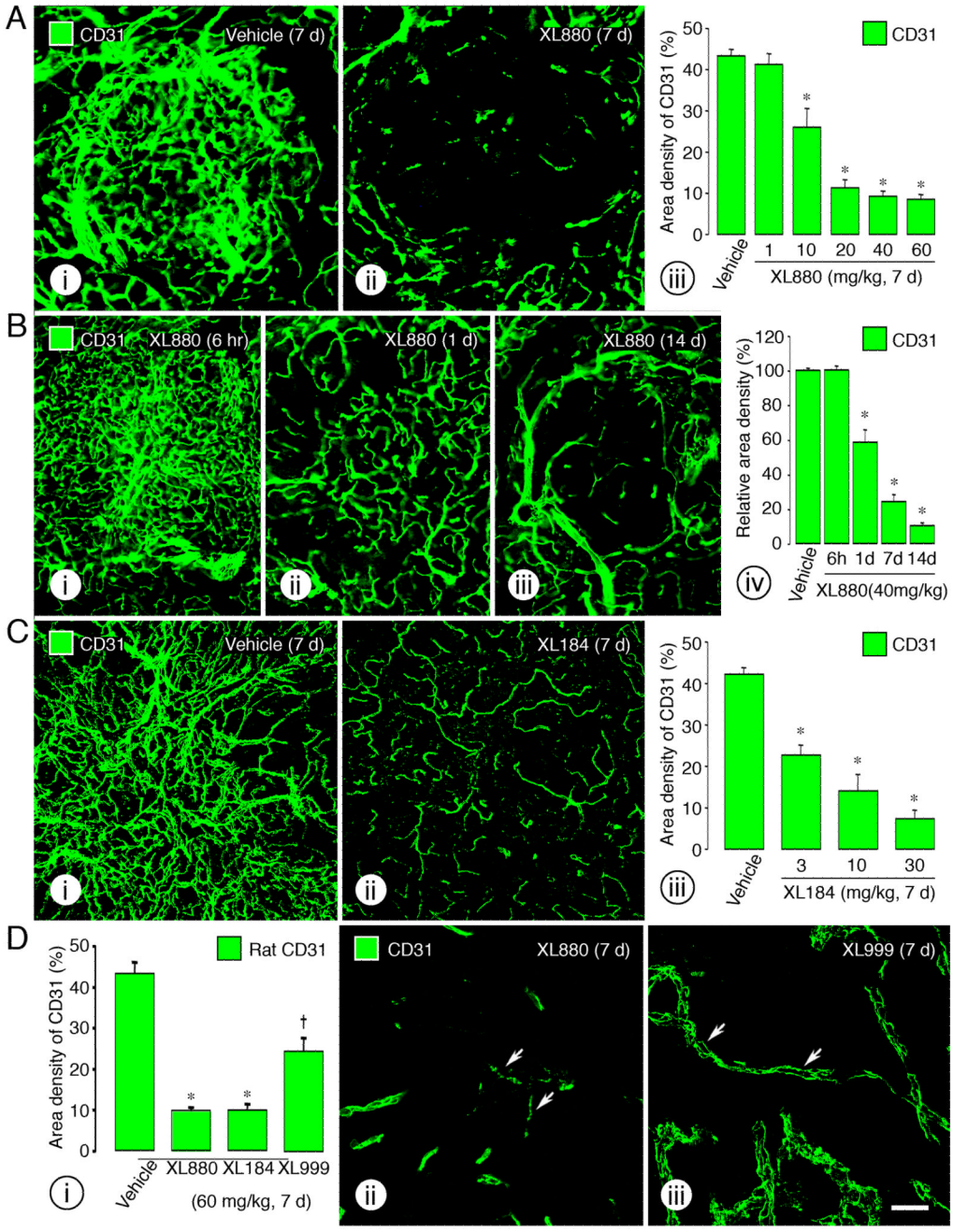

Figure 1. XL880, XL184, and XL999 effects on tumor vessels

Fluorescence micrographs compare the vasculature of RIP-Tag2 tumors stained for CD31 immunoreactivity. **Ai–ii**, vascularity is conspicuously greater after vehicle than after XL880 (60 mg/kg) for 7 days. **Aiii**, dose-response of tumor vessel regression after XL880 for 7 days. **Bi–Biii**, no reduction of vascularity at 6 hr after XL880 (40 mg/kg) but conspicuous reductions after 1 day or 14 days. **Biv**, time-course of reduction in tumor vascularity after XL880. **Ci–Cii**, reduction in vascularity after XL184 (30 mg/kg) for 7 days. **Ciii**, dose-response after XL184 for 7 days. **Di**, smaller reduction in vascularity after XL999 than after XL880 or XL184. **Dii**, narrow, irregular, or fragmented tumor vessels (arrows) still present after XL880 or XL184 for 7 days. **Diii**, larger and less tortuous tumor vessels (arrows)

remain after XL999 for 7 days. * $P < 0.001$ vs. vehicle. † $P < 0.001$ vs. XL880 and XL184. Scale bar: 120 μm (**A, B, C**); 30 μm (**D**).

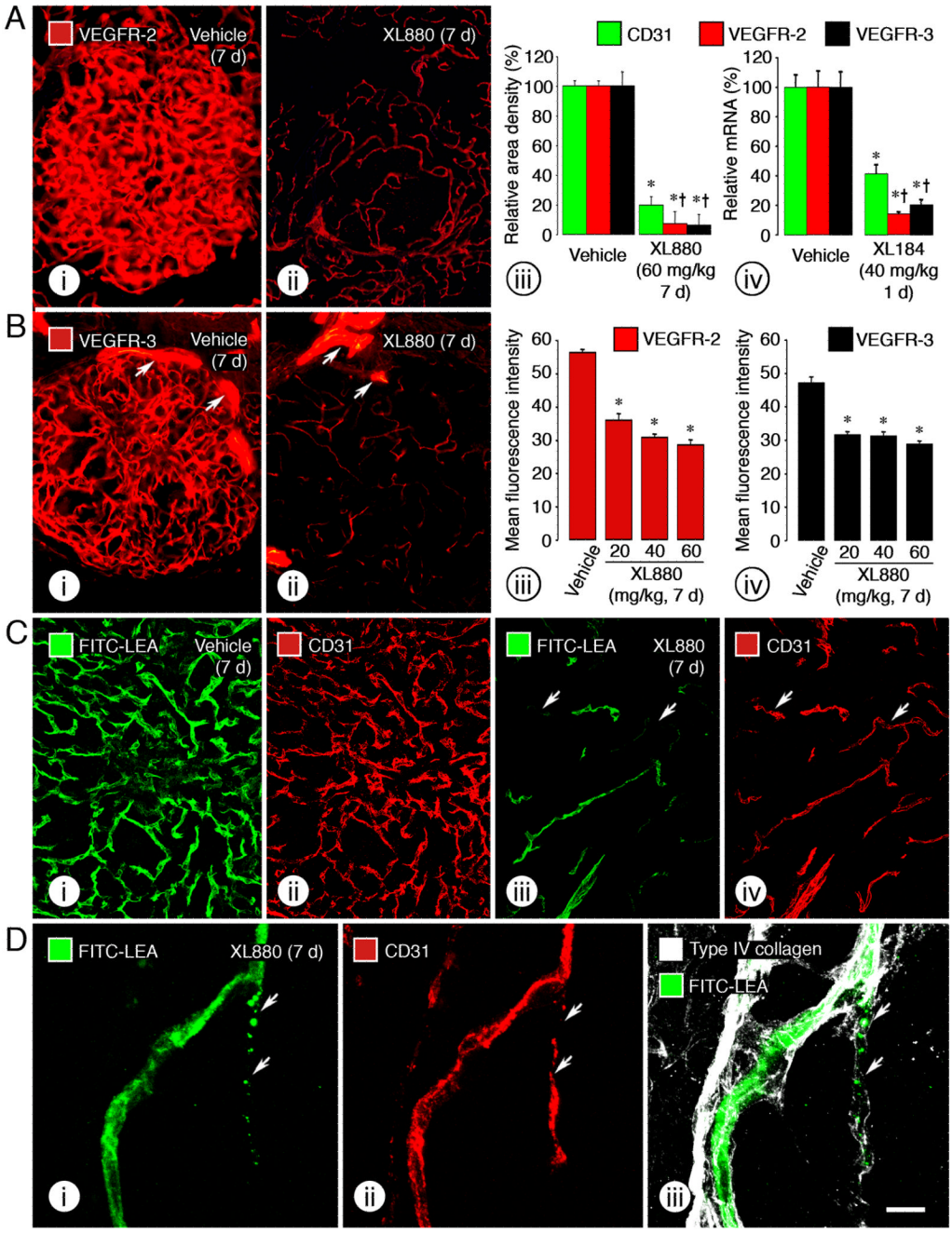

Figure 2. VEGFR-2 and VEGFR-3 expression and vessel function

Confocal micrographs of RIP-Tag2 tumors. **Ai**, strong VEGFR-2 immunoreactivity after vehicle. **Aii**, weak VEGFR-2 after XL880 for 7 days. **Aiii**, reductions in CD31, VEGFR-2 and VEGFR-3 immunoreactivities after XL880 (60 mg/kg, 7 days). **Aiv**, significantly reduced expression of VEGFR-2 and VEGFR-3 mRNA after XL184 (40 mg/kg, 1 day) compared to smaller reduction in CD31 mRNA. **Bi**, strong VEGFR-3 staining in tumor vessels and lymphatics (arrows) after vehicle. **Bii**, markedly reduced VEGFR-3 in tumor vessels but not in lymphatics (arrows) after XL880. **Biii–iv**, dose-dependent reductions in fluorescence intensity of VEGFR-2 and VEGFR-3 in tumor vessels after XL880. **Ci–iv**, tumor vessel function, assessed by i.v. injection of FITC-LEA lectin (green) followed by

staining for CD31 (red). All tumor vessels have lectin staining (uniform perfusion) after vehicle, but scattered tumor vessels lack lectin staining (non-perfused vessels, arrows) after XL880. **Di–iii**, discontinuities in staining for lectin (arrows), CD31 (arrows), and basement membrane (arrows) after XL880. * $P < 0.001$ vs. vehicle. † $P < 0.001$ vs. corresponding CD31. Scale bar: 120 μm (**A, B**); 60 μm (**C**); 10 μm (**D**).

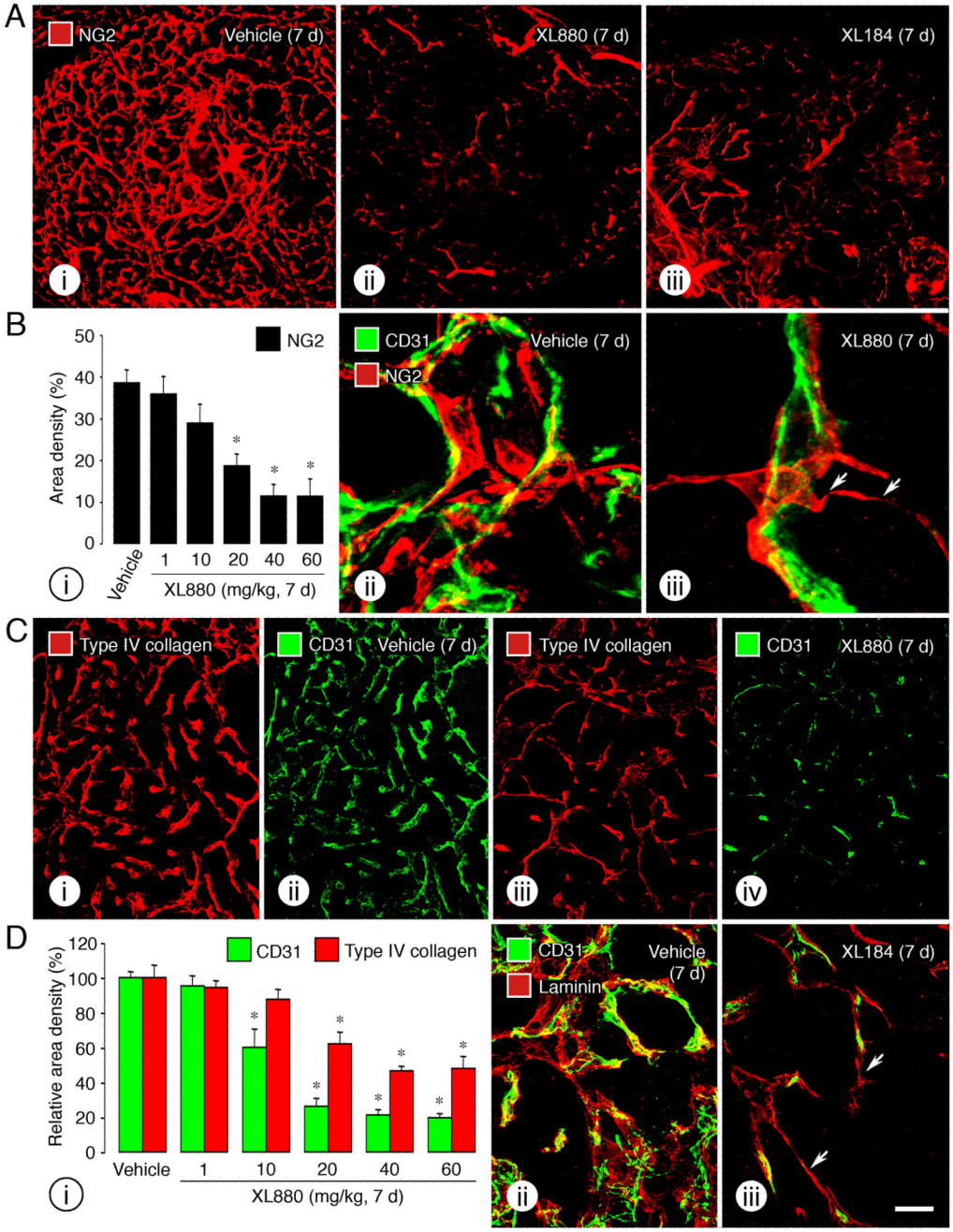

Figure 3. Reduction in pericytes and basement membrane sleeves

Confocal micrographs of RIP-Tag2 tumors. **Ai**, abundant NG2-positive tumor vessels after vehicle, reflecting abundance of pericytes. **Aii–iii**, sparse staining for NG2 after XL880 or XL184. **Bi**, dose-dependent NG2 reduction after XL880. **Bii–iii**, loose association of NG2-positive pericytes after vehicle or XL880 for 7 days (40 mg/kg, arrows). **Ci–iv**, type IV collagen (red) and CD31 (green) in tumors after vehicle or XL880. **Di**, dose-dependent decrease in type IV collagen after XL880 compared to larger reductions in CD31. Differences in amounts of type IV collagen and CD31 reflect the abundance of empty basement membrane sleeves. **Dii–iii**, tumor vessels stained for laminin (red) and CD31 (green) showing more abundant empty basement membrane sleeves after XL184 (arrows).

Dose of XL880 or XL184, 60 mg/kg for 7 days. * $P < 0.001$ vs. vehicle. Scale bar: 120 μm (**A**); 10 μm (**B**); 60 μm (**C**); 30 μm (**D**).

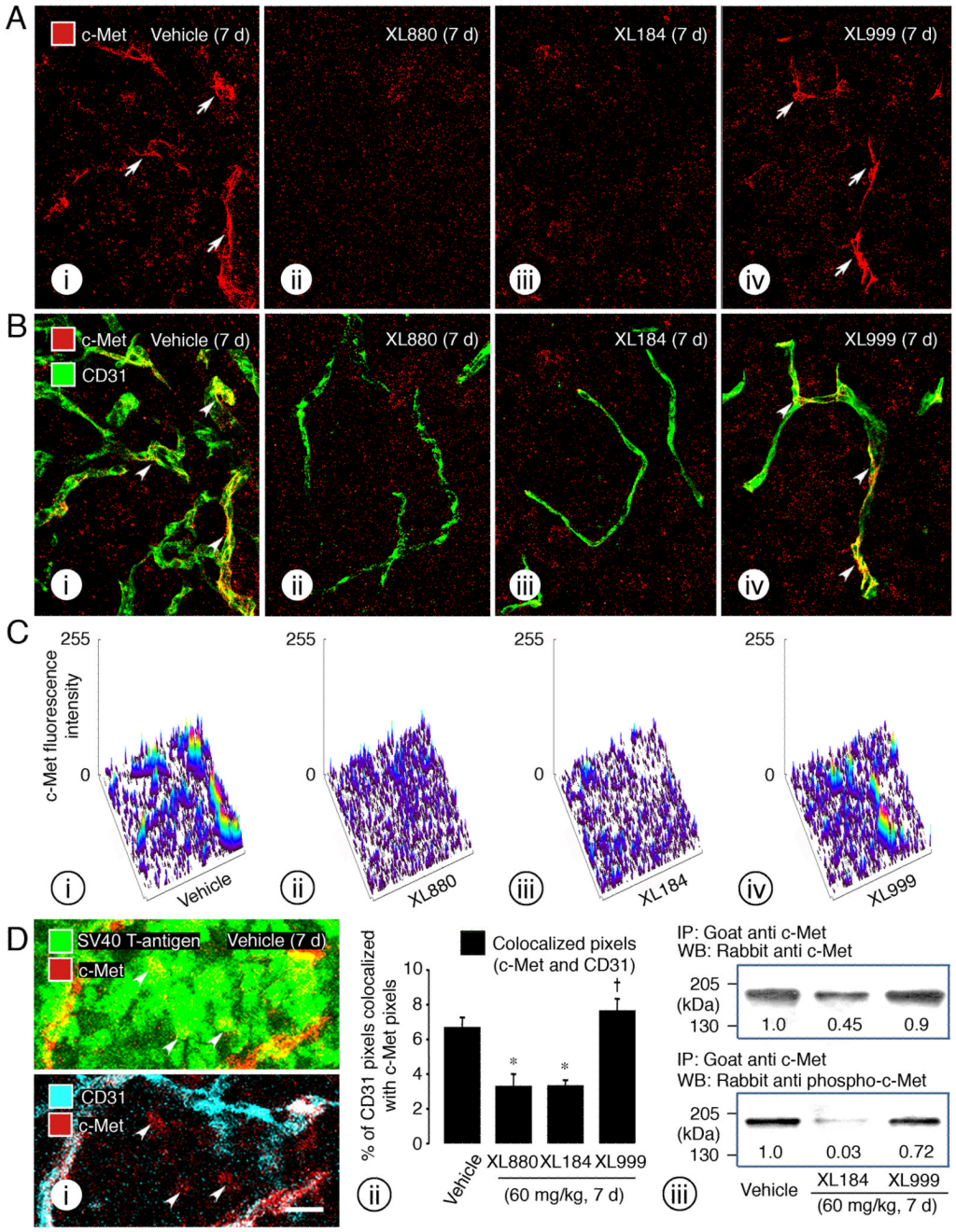

Figure 4. c-Met immunoreactivity and expression in RIP-Tag2 tumors

Ai–Aiv, confocal micrographs show the vascular pattern of c-Met immunoreactivity (red, arrows) after vehicle or after XL999 but little or no vascular staining after XL880 or XL184. **Bi–iv**, same images as in **Ai–iv**, shown here with the CD31 channel (green) added, show the colocalization of CD31 with c-Met immunoreactivity after vehicle or XL999 (arrowheads) but not after XL880 or XL184. **Ci–iv**, surface plots of c-Met immunofluorescence intensity show peaks that coincide with tumor vessels after vehicle or XL999, and confirm the reduction in c-Met immunofluorescence of tumor vessels after XL880 or XL184. **Di**, confocal micrographs show the presence of c-Met immunoreactivity (red) in some RIP-Tag2 tumor cells (green, SV40 T-antigen, arrows) and in tumor vessels (cyan, CD31) after

vehicle. **Dii**, measurements show decrease in CD31 pixels colocalized with c-Met pixels after XL880 or XL184 but not after XL999. **Diii**, immunoblots show large reduction in phosphorylated c-Met after XL184 but not after XL999. Dose of XL compounds was 60 mg/kg for 7 days. * $P < 0.001$ vs. vehicle. † $P < 0.001$ vs. XL880 and XL184. Scale bar: 30 μm (**A, B**) and 10 μm (**D**).

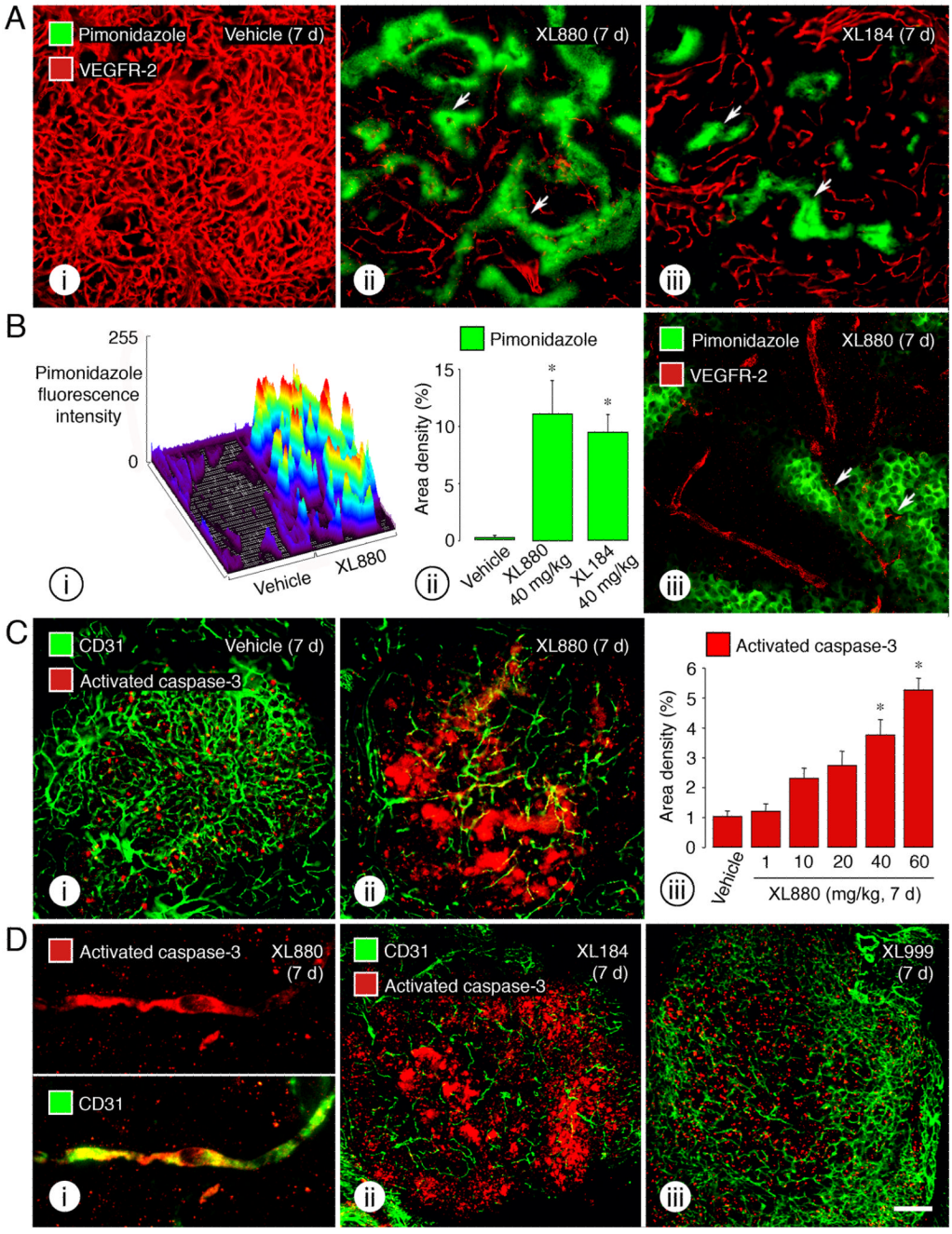

Figure 5. Hypoxia and apoptosis in RIP-Tag2 tumors

Ai–iii, confocal micrographs of RIP-Tag2 tumors stained for VEGFR-2 (red, endothelial cells) and pimonidazole (green, hypoxia) show that the amount and distribution of hypoxia (arrows) increased from none after vehicle to widespread after XL880 or XL184 (40 mg/kg) for 7 days. **Bi**, surface plot of pimonidazole fluorescence was essentially flat after vehicle but had high peaks after XL880. **Bii**, measurements of fractional area of pimonidazole staining in tumors. **Biii**, some regions of pimonidazole staining overlapped fragmented tumor vessels (arrows) but most were separated from tumor vessels by sleeves of unstained tumor cells (dark). **Ci**, scattered apoptotic cells identified by activated caspase-3 staining in tumors after vehicle. **Cii**, widespread and clumped activated caspase-3 staining in tumors

after XL880 (60 mg/kg) for 7 days. **Ciii**, dose-response increase of activated caspase-3 staining of tumors after XL880 for 7 days. **Di**, apoptotic endothelial cells in tumor vessel stained for activated caspase-3 (upper) and colocalized with CD31 (lower) after XL880 for 7 days. **Dii–iii**, widespread activated caspase-3 immunoreactivity after XL184 but not after XL999 (40 mg/kg) for 7 days. * $P < 0.001$ vs. vehicle. Scale bar: 120 μm (**A, C**); 30 μm (**B**); 10 μm (**Di**); 240 μm (**Dii–iii**).

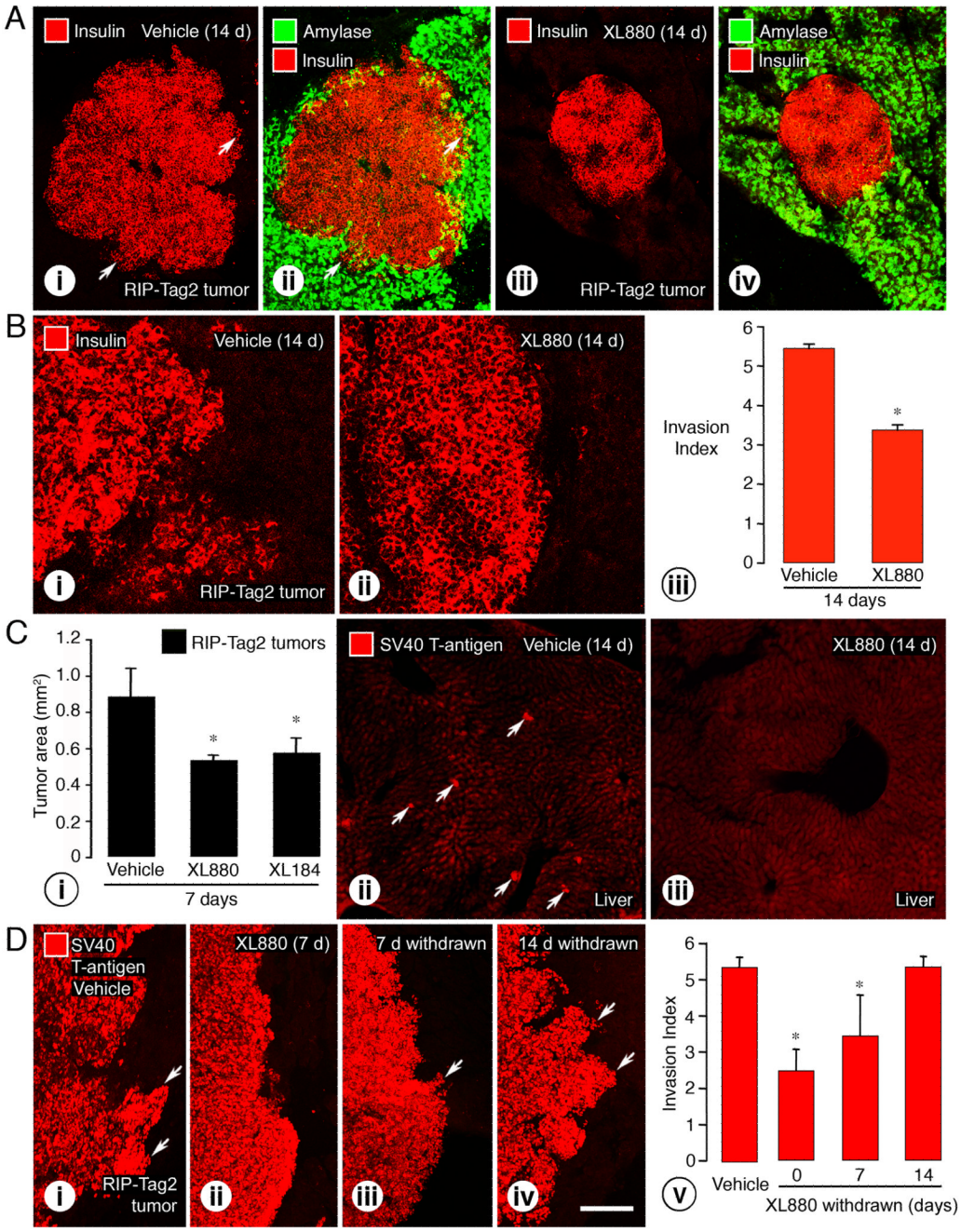

Figure 6. Treatment-related differences in tumor invasiveness, size, and liver metastases

Confocal micrographs of RIP-Tag2 tumors. **Ai–ii**, irregular border (arrows) of tumor after vehicle. **Aiii–iv**, smooth contour of tumor after XL880 for 14 days. Tumor cells stained for insulin (red) and surrounding exocrine pancreas stained for amylase (green). **Bi–iii**, measurements show significant reduction in irregularity of tumor border, reflected by Invasion index, after XL880 for 14 days. **Ci**, measurements of histological sections show significant reductions in size of RIP-Tag2 tumors after treatment with XL880 (40%) or XL184 (35%) for 7 days, from age 10 to 11 weeks. **Cii–iii**, scattered tumor cells (arrows) marked by SV40 T-antigen immunoreactivity are shown in the liver of 12-week-old RIP-Tag2 mouse after vehicle, but no stained cells after XL880 for 14 days. **Di**, irregular tumor

border after vehicle (arrows). **Dii**, smoother tumor border after XL880 for 7 days. **Diii**, smooth border with small projects at 7 days after withdrawal of XL880 (arrows). **Div**, greater irregularity of tumor border (arrows) at 14 days, which is similar to but not more severe than baseline. **Dv**, Invasion index measurements show the magnitude of changes in tumor border irregularity before and after withdrawal. * $P < 0.05$ vs. vehicle. Scale bar: 150 μm (**A**); 55 μm (**B**); 180 μm (**C**); 50 μm (**D**).

Table 1

IC_{50} (nM) values of XL880, XL184, XL999 and sorafenib on kinase activity

Kinases	VEGFR-2 (KDR)	c-MET (HGFR)	FGFR1	PDGFR-β	KIT	FLT1	FLT4	FLT3	Tie2	AXL	RON
XL880 (27, 31)	0.86	0.4	660	9.6	6.7	6.8	2.8	3.6	1.1	11	3
XL184 (29, 32)	0.035	1.3	5294	234	4.6	12	6.0	11.3	14.3	7.0	124
XL999 (33, 34)	2.6	463	8.2	1.5	13.8	29	3.0	0.8	270	4.6	124
Sorafenib (50)	90	–	580	57	68	–	–	33	–	–	–

IC_{50} values (nM) for inhibition of phosphorylation of 11 receptor tyrosine kinases by XL880, XL184, and XL999 show similarities for VEGFR-2, KIT, and AXL and differences for c-MET. XL880 and XL184 differ in inhibition of PDGFR-β and RON, and neither inhibits FGFR1. IC_{50} values of sorafenib are shown for comparison.